Available online at www.sciencedirect.com
SCIENCE DIRECT®
Journal of Nuclear Materials 336 (2005) 279–290
journal of nuclear materials
www.elsevier.com/locate/jnucmat

Low temperature creep crack growth in low alloy reactor pressure vessel steel

Rui Wu *, Rolf Sandström, Facredin Seitisleam

Swedish Institute for Metals Research, Drottning Kristinas väg 48, S-l 14 28 Stockholm, Sweden

Received 15 March 2004; accepted 6 October 2004

Abstract

Uni-axial creep and creep crack growth (CCG) tests between 320 °C and 420 °C have been carried out in a low alloy reactor pressure vessel steel (ASTM A508 class 2). Both as-received material and simulated coarse grained heat affected zone (CGHAZ) microstructure have been tested. CCG does occur at tested temperatures. The lifetimes for the CCG tests are considerably shorter than those for the uni-axial creep tests at the same reference stress and temperature. This is more pronounced at longer lifetimes or lower stresses. Increasing temperature causes a significant reduction of lifetime, e.g. the CCG lifetime on the simulated CGHAZ is reduced by a factor of five as temperature raises from 320 °C to 340 °C at given reference stresses. Three distinct regions relating crack length and time are observed for the CCG tests. After incubation, the crack grows steadily until it accelerates to approach failure. For the longer time CCG tests, the cracks propagate intergranularly, independent of temperature and microstructure. An approximate linear extrapolation based on the stress–time results indicates that the reference stress causing failure in the simulated CGHAZ due to CCG at a given lifetime of 100 000 h at 320 °C is lower than both yield and tensile strengths, showing that the design stress should be based on creep crack growth property rather than static strength.

1. Introduction

Failures due to low temperature creep crack growth (LTCCG) have been reported world-wide. They have been observed after service lives from 8000 to 100 000 h in conventional fossil fired power plants at around 360 °C [1–4]. Investigations showed that crack growth had taken place a long period of time before failure.

In a previous study the creep and creep crack growth (CCG) behaviour was investigated in an ASTM A508 low alloy reactor pressure vessel steel as well as simulated coarse grained heat affected zone (CGHAZ) microstructures across a weldment at 360 °C [5]. The results show that (1) CCG does occur, (2) shorter lifetimes are found in the CCG tests in comparison to the uni-axial creep tests at the same reference stress, (3) for the CCG tests the lifetime in the simulated CGHAZ is shorter than that in the as-received parent material at longer rupture times, and (4) intergranular (brittle) rupture dominates in the simulated CGHAZ. These effects have also been studied with notched tensile creep tests for the parent material [6].

Question arises whether there is CCG at even lower temperatures than 360 °C since this steel and its weldment are usually operating at temperatures of approximately 290–320 °C. At such low temperatures, which are far below the limit temperature for design against

* Corresponding author. Tel.: +46 8 440 48 09; fax: +46 8 440 45 35.
E-mail address: rui.wu@simr.se (R. Wu).

0022-3115/$ - see front matter © 2004 Elsevier B.V. All rights reserved.
doi:10.1016/j.jnucmat.2004.10.001

creep for this steel, design stresses in power generating application are traditionally based on tensile properties, and creep is generally considered to be of little importance, see for example [7].

Not only the shortest lifetime but also brittle failure was observed in the simulated CGHAZ, indicating that coarse grained HAZ is a weak and risky link in a weld joint. There are various ways to produce the coarse grained HAZ; for instance by welding and by simulating. Advantages of simulation are to (i) provide representative welding parameters, (ii) reduce scatter in testing results caused by inhomogeneities in real weldment, and (iii) increase the degree of homogeneity which facilitates the study of CCG and damage development. However, effects of microstructural discontinuity, local property gradient and welding residual stresses cannot be considered.

By simulating the microstructure found in the coarse grained HAZ of ASTM A508 low alloy reactor pressure vessel steel, this project aims at (i) studying creep and CCG behaviour between 320 °C and 420 °C, (ii) investigating creep damage, and (iii) performing data comparison and analysis.

2. Material and experiments

2.1. As-received material

A low alloy reactor pressure vessel steel bar (ASTM A508 class (2) was used. It is composed of pearlite and ferrite, see Fig. 1(a). Hardness (HV10) is 185 and grain size is 21 μm. The chemical compositions of the test material and requirements of ASTM [8], are shown in Table 1.

2.2. Simulation of coarse grained heat affected zone (CGHAZ)

To simulate CGHAZ microstructure across a weldment, the as-received material was heat treated at 1150 °C for 30 min, cooled in boiling water, tempered at 640 °C for 2 h, followed by furnace cooling. After heat treatment, the microstructure is composed of tempered martensite, see Fig. 1(b). Hardness (HV10) is 429 and grain size is 144 μm.

2.3. Hot tensile tests

Hot tensile tests were performed at 320 °C and 340 °C for both as-received material and the simulated CGHAZ at a deformation velocity of 0.0001/s. The results are given in Table 2.

2.4. Uni-axial and compact tension (CT) specimens

Uni-axial creep specimens were longitudinally taken from the bar. The specimens are cylindrical with threaded ends with 5 mm diameter and 50 mm gauge length.

Standard CT specimens were used in the CCG testing. The geometry of the CT specimens is shown in Fig. 2. The spark machined notch has a root radius of 0.15 mm. The notch is oriented along the transverse

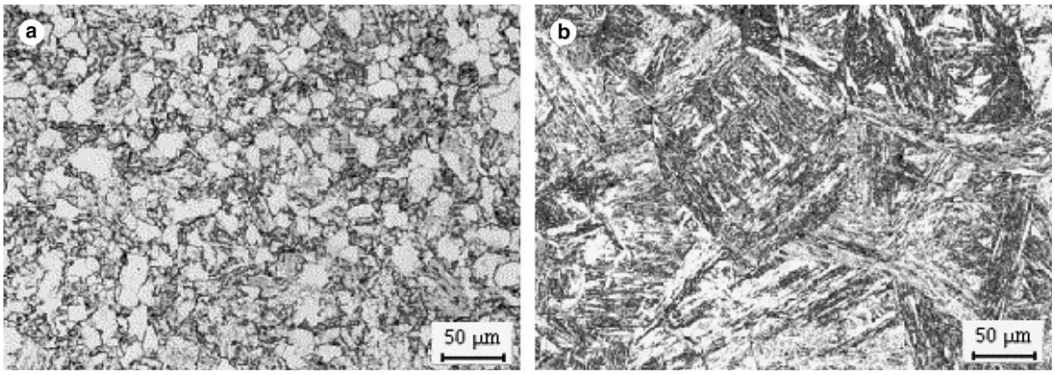

Fig. 1. Pre-metallography showing microstructure of (a) as-received material, and simulate CGHAZ.

Table 1
Chemical compositions (wt%)

Material	C	Si	Mn	S	P	Cr	Mo	Ni
As-received	0.19	0.29	0.69	0.0087	0.012	0.35	0.63	0.84
ASTM A508 class 2	⩽0.27	0.15–0.40	0.50–1.00	⩽0.025	⩽0.025	0.25–0.45	0.55–0.70	0.50–1.00

Table 2
Hot tensile testing results

Temperature, °C	Yield stress, MPa		Tensile stress, MPa		Elongation at rupture, %		Reduction of area at rupture, %	
	As-received	Simulated CGHAZ	As-received	Simulated CGHAZ	As-received	Simulated CGHAZ	As-received	Simulated CGHAZ
320	306	614	529	756	17.7		56.4	
340	298	614	525	751	17.5	10.5	49.2	46.7
360			519	771				
420				672				

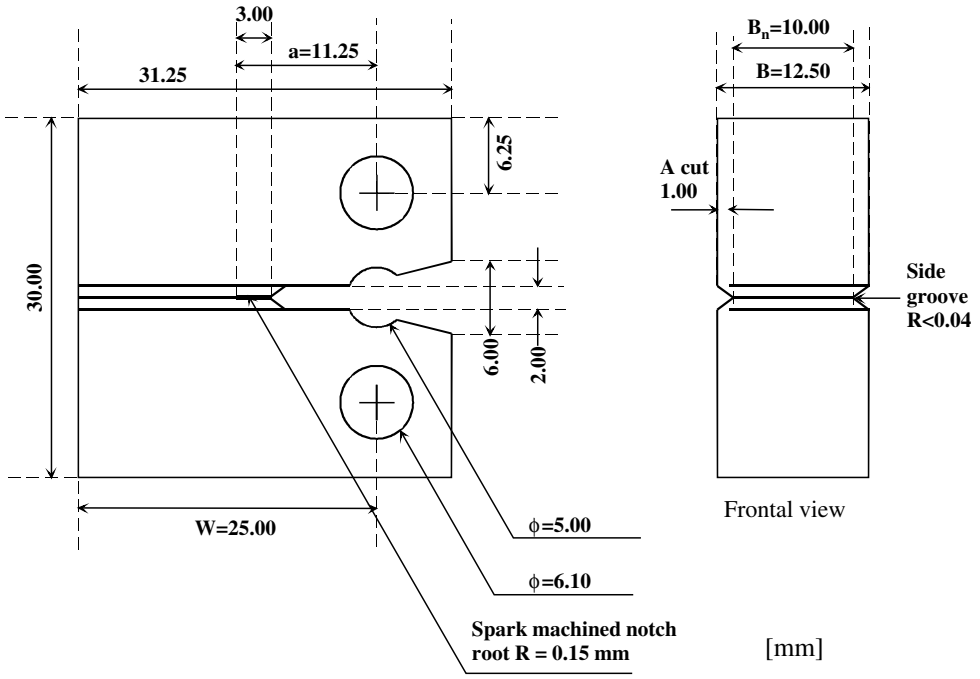

Fig. 2. Standard compact tension (CT) specimen geometry.

section of the bar, which allows the crack to grow in the radius direction. The side grooves promote uniform crack extension across the thickness of the specimen.

2.5. Creep and CCG tests

By using single specimen, constant load creep testing machines the uni-axial creep specimens from simulated CGHAZ were tested between 320 °C and 360 °C.

The CCG tests follow the instructions described in the standard ASTM E-1457 [9]. The tests between 320 °C and 420 °C were conducted for both as-received material and simulated CGHAZ in a dead-weight lever creep test rig equipped for CCG testing. The direct current potential drop method was used to monitor crack progress and a purpose-built extensometer was used to measure load line displacement (LLD).

All the creep and crack growth tests were carried out in air and progressed to final rupture. The PD output and the LLD for the CCG tests, the creep strain for the uni-axial creep tests as well as temperatures were recorded periodically by a logger. The maximum temperature variations during test were controlled within ±2 °C of the testing temperatures.

The reference stress for CCG tests, σ_{ref}, is calculated according to

$$\sigma_{\text{ref}} = \frac{P}{M \cdot B_{\text{eq}} \cdot W}, \tag{1}$$

where

$$M = -\left(1 + \gamma\left(\frac{a}{W}\right)\right) + \sqrt{(1+\gamma)\left(\gamma\left(\frac{a}{W}\right)^2 + 1\right)} \tag{1a}$$

and

$$B_{\mathrm{eq}} = B - \frac{(B - B_n)^2}{B} \tag{1b}$$

and

$$\gamma = \frac{2}{\sqrt{3}}, \tag{1c}$$

where P is the load in N, a, w, B and B_n are shown in Fig. 2. The choice of M is based on the assumption of plane stress condition.

2.6. Post test metallography

Uni-axial creep and CT specimens were metallographically examined using light optical microscope (LOM). At mid-thickness perpendicular to the fracture, the specimens were sectioned, ground and polished to 1 μm grit level before etching in 4% nital.

Fractography was performed on CT specimens using scanning electron microscopy (SEM). Prior to examination, the fracture was ultrasonically cleaned.

After failure, the maximum accumulated crack growth length at rupture $\Delta a_{\max}$ on the CT specimens was measured using stereo microscope.

3. Results

3.1. Uni-axial creep tests

Creep curves at 320 °C, 340 °C and 360 °C are shown in Fig. 3(a), (b) and (c), respectively. Some tests were interrupted after minimum creep strain rate was approached. It can be seen that creep curves show insignificant primary creep, dominant secondary creep and pronounced tertiary creep. Time to failure t_{R} versus stress σ is given in Fig. 4. t_{R} is sensitive to both temperature and stress, e.g. as temperature is reduced from 340 °C to 320 °C, time to rupture increases from 388 h to 19 991 h at 715 MPa. In the double logarithmic scales t_{R} increases linearly with decreasing σ at given temperatures and this relation can be described as

$$t_{\mathrm{R}} = \eta' \sigma^{-\eta}, \tag{2}$$

where η' and η are empirically determined constants. η is about 97 at 340 °C and 168 at 360 °C.

t_{R} versus elongation at rupture is exhibited in Fig. 5. Elongation at rupture is about 8% for all the ruptured tests, insensitive to temperature and time. Minimum creep strain rate $\dot{\varepsilon}_{\min}$ versus stress σ is given in Fig. 6. $\dot{\varepsilon}_{\min}$ decreases with decreasing σ. In the double logarithmic scales the $\dot{\varepsilon}_{\min} - \sigma$ relation follows the Norton's law

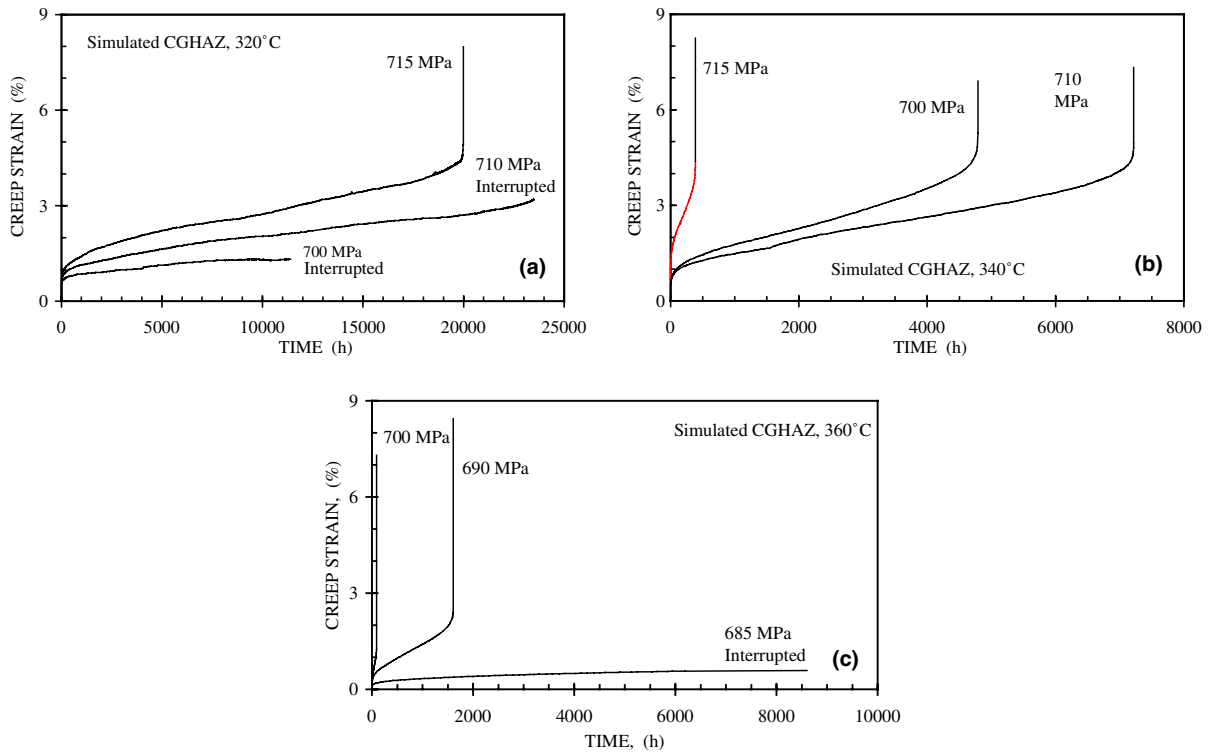

Fig. 3. Creep strain versus time for uni-axial creep tests in simulated CGHAZ at (a) 320 °C, (b) 340 °C and (c) 360 °C.

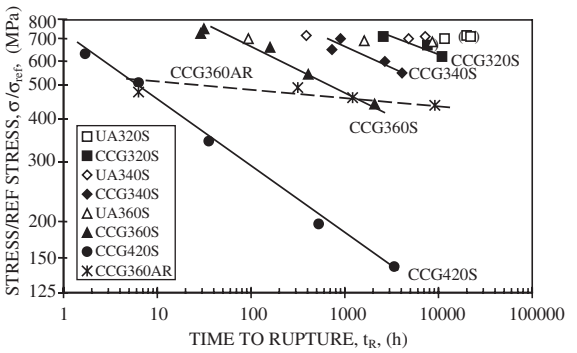

Fig. 4. Stress for uni-axial (UA) or reference stress for CCG tests versus time to rupture between 320 °C and 420 °C. Results in brackets mean interrupted tests. S refers to simulated CGHAZ and AR as-received material.

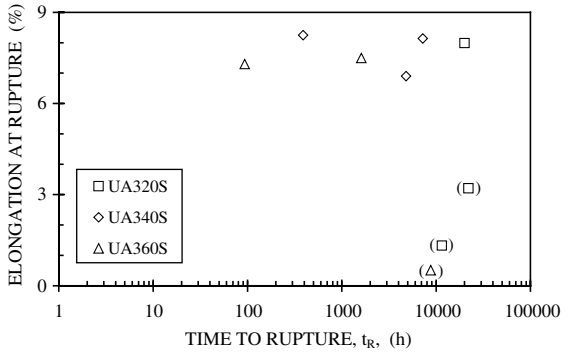

Fig. 5. Elongation at rupture versus time to rupture for uni-axial creep tests. Results in brackets mean interrupted tests.

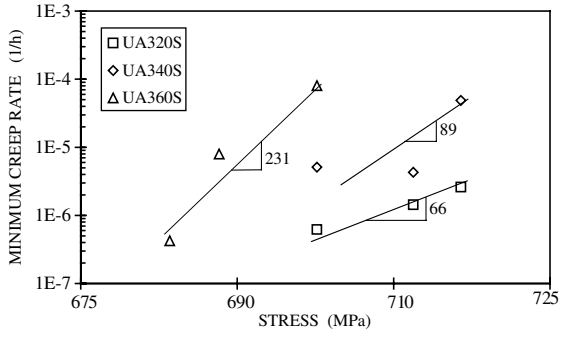

Fig. 6. Minimum creep strain rate versus stress for uni-axial creep tests.

$$\dot{\varepsilon}_{\min} = b\sigma^n, \tag{3}$$

where b is constant and n the stress exponent, n is 66 at 320 °C, 89 at 340 °C, and 231 at 360 °C.

3.2. Creep crack growth (CCG) tests

t_R versus reference stresses σ_{ref} for the CCG tests is also shown in Fig. 4, in comparison to the uni-axial creep testing results. t_R in the CCG tests includes both initiation time and growth time all the way to failure. It can be seen from Fig. 4 that

1. CCG does occur at given temperatures and tested microstructures.
2. CCG lifetimes are significantly shorter than the uni-axial lifetimes, especially at lower stresses.
3. Log t_R increases linearly with decreasing log σ_{ref} at a given temperature. This is valid for both the as-received material and the simulated CGHAZ.
4. For the simulated CGHAZ, a temperature increase from 320 °C to 340 °C, from 320 °C to 360 °C and from 320 °C to 420 °C reduces t_R by a factor of about 5, 17 and 35, respectively.
5. At 360 °C the as-received material gives shorter lifetimes than the simulated CGHAZ at higher σ_{ref}. But, this tends to be reversed at lower σ_{ref}, or longer lifetimes.

From Fig. 4 it is obvious that the t_R–σ_{ref} relations for both the as-received material and the simulated CGHAZ obey also Eq. (2) at given temperatures

$$t_R = \alpha'(\sigma_{ref})^{-\alpha}, \tag{4}$$

where α' and α are empirically determined constants. For the simulated CGHAZ α is 10.3 at 320 °C, 10.9 at 340 °C, 8.3 at 360 °C, and 5.3 at 420 °C. For the as-received material α is 41 at 360 °C.

The accumulated crack length Δa as a function of time t at given σ_{ref} is shown in Fig. 7 for the tests at 320 °C. The Δa–t relations obtained at other temperatures are analogous to that at 320 °C. Δa is calculated according to an analytical solution recommended by the standard ASTM E-1457 [9–11]

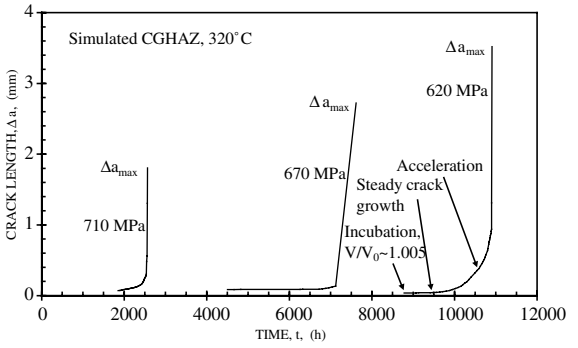

Fig. 7. Calculated accumulated crack length versus time for simulated CGHAZ at 320 °C.

$$\Delta a = \frac{2W}{\pi}\cos^{-1}\left\{\frac{\cosh(\pi Y_0/2W)}{\cosh\left[\frac{V}{V_0}\cosh^{-1}\left(\frac{\cosh(\pi Y_0/2W)}{\cos(\pi a_0/2W)}\right)\right]}\right\} - a, \tag{5}$$

where a is the initial crack length in mm with respect to the initial voltage V_0 at time $t = 0$, V the output voltage at t and Y_0 the half distance between the output voltage leads in mm. The values of W and a are shown in Fig. 2. Y_0 is 2.5 mm in the present case. The maximum accumulated crack length at rupture Δa_{max} shown in Fig. 7 is the measured values. Δa_{max} was determined by observing fracture surface where the crack growth zone was heavily oxidised and fracture patterns were different in different zones, cf. Fig. 8.

It can be seen from Fig. 7 that after a long incubation period, in which no apparent crack growth could be observed, the crack propagated steadily before it accelerated to approach the rupture. In the Fig. 7 arrows are given to identify the various regions. Significant crack growth took place at later stage of the tests. Δa_{max} increases with time. Increasing temperature and testing time result in a larger Δa_{max}.

Crack growth rate $\dot{a}$ (also written as da/dt) as a function of creep fracture parameter C^* for the simulated CGHAZ is shown in Fig. 9(a) for the tests at 320 °C and in Fig. 9(b) for the tests at 340 °C, respectively. The $\dot{a} - C^*$ relations at 360 °C and 420 °C are similar to those at 320 °C and 340 °C. $\dot{a}$ is simply the slope of a straight line connecting two adjacent data points (Δa_{i+1} and Δa_i and corresponding time t_{i+1} and t_i) on the Δa–t curves and can be defined as

$$\dot{a} = \frac{\Delta a_{i+1} - \Delta a_i}{t_{i+1} - t_i}. \tag{6}$$

In the case of CT specimen the following expression is well accepted for the estimation of C^* [9,12]

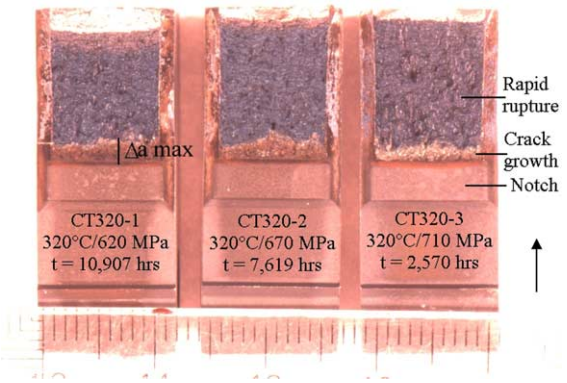

Fig. 8. LOM image showing fracture surface of CT specimens at 320 °C. The length of Δa_{max} is schematically shown. Arrow indicates the crack growth direction.

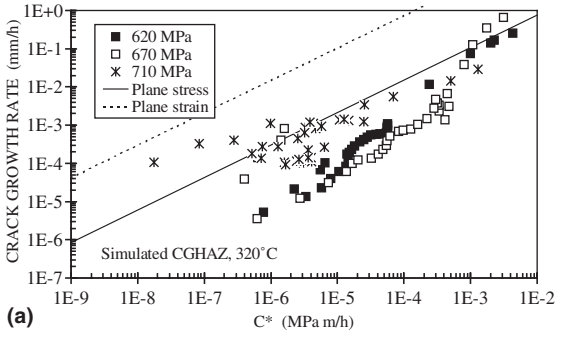

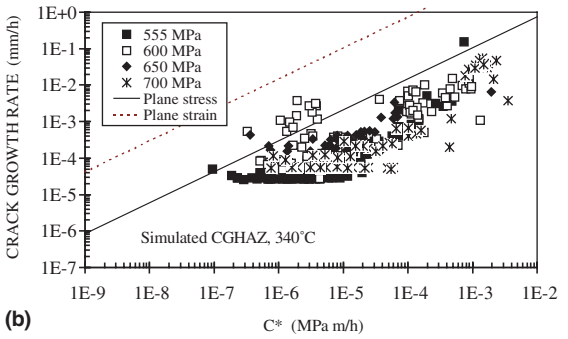

Fig. 9. Creep crack growth rate versus creep fracture parameter C^* at (a) 320 °C and (b) 340 °C. Lines by Eq. (8) are included.

$$C^* = \frac{P \cdot \dot{V}_c}{B(W-a)}\left[\frac{n}{n+1}\left(2 + 0.522\frac{W-a}{W}\right)\right], \tag{7}$$

where C^* is in MPa m/h, P is the applied load in N, $\dot{V}_c$ the load line displacement rate due to creep in mm/h, and n the stress index in Norton's law. The calculations of $\dot{V}_c$ and other parameters are shown in Appendix A.

Fig. 9 also includes an empirical expression relating $\dot{a}$ and C^* [13]

$$\dot{a} = \frac{\psi \cdot C^{*0.85}}{\varepsilon_R}, \tag{8}$$

where ε_R is the uni-axial creep ductility at rupture at relevant temperature. The coefficient ψ is described in [13] and contains a factor that varies with the stress/strain state. ψ is 3 for plane stress and 150 for plane strain. Lines by Eq. (8) are included in Fig. 9 to give an appreciation of the stress state at the crack tip.

It is clear from Fig. 9 that at steady crack growth region where $\dot{a}$ is constant, C^* increases monotonically. At crack acceleration region C^* increases fairly linearly with increasing $\dot{a}$ in the double logarithmic scales and this relation takes the form of

$$\dot{a} = D_0(C^*)^{\phi}, \tag{9}$$

where D_0 and ϕ are constants. ϕ ranges from 0.5 to 1 for the simulated CGHAZ. This is independent of temperatures. For the as-received material at 360 °C, ϕ is slightly

larger than unity. Fig. 9 also shows that $\dot{a}$–C^* plots lie closer to the plane stress state line than to the plane strain line proposed by Eq. (8).

The maximum accumulated crack length at rupture Δa_{max} as a function of time to rupture t_R is shown in Fig. 10 for all the CCG tests. It is clear that Δa_{max}–t_R relation is temperature and time dependent. At the same time, the higher the temperature, the larger the Δa_{max}. At the same temperature, the longer the t_R, the larger the Δa_{max}.

Relations between steady crack growth rate $\dot{a}_S$ and reference stress σ_{ref} as well as between $\dot{a}_S$ and t_R are also found. $\dot{a}_S$–σ_{ref} relation is shown in Fig. 11 for all the CCG tests. It is seen that $\dot{a}_S$ is higher at higher temperature at the same σ_{ref}. In the double logarithmic scales a_S decrease linearly with decreasing σ_{ref}. This power-law relation is analogue to the Norton's law for the uni-axial creep behaviour, cf. Fig. 6

$$\dot{a}_S = v'(\sigma_{ref})^v, \tag{10}$$

where v' and v are constant and reference stress index, respectively, v decreases with increasing temperature

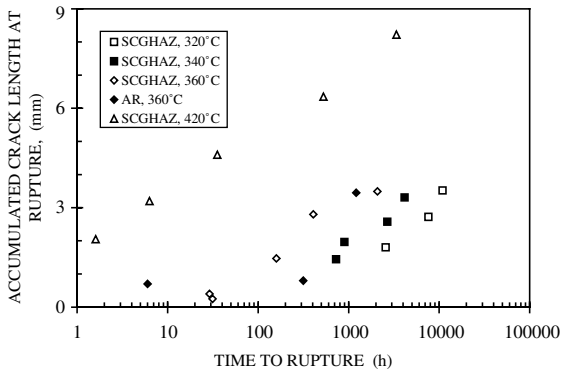

Fig. 10. Maximum accumulated crack length at rupture versus time to rupture. SCGHAZ refers to simulated CGHAZ and AR as-received material.

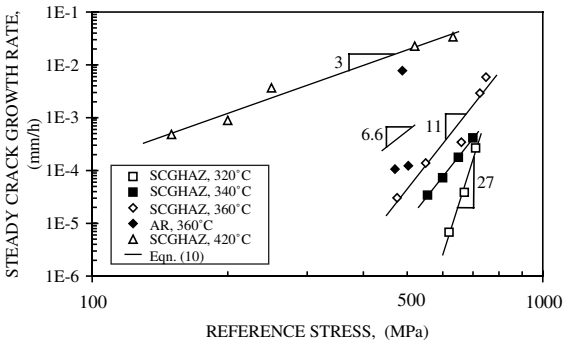

Fig. 11. Steady crack growth rate versus reference stress for all the CCG tests. Eq. (10) is included.

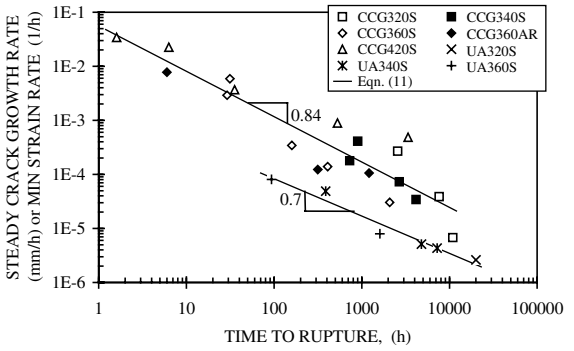

Fig. 12. Steady crack growth rate for the CCG tests and minimum creep strain rate for the uni-axial creep tests versus time to rupture. Eq. (11) is included.

for the simulated CGHAZ. For example, v is 27 at 320 °C, 11 at 340 °C and 360°, and 3 at 420 °C. For the as-received material at 360 °C, v is 6.6. However, scatter in $\dot{a}_S$–σ_{ref} relation for the as-received material is seen.

$\dot{a}_S$ is plotted against t_R in Fig. 12 for all the CCG tests. In Fig. 12 also includes uni-axial creep results where t_R is plotted against the minimum creep strain rate $\dot{\varepsilon}_{min}$. It is noted that $\dot{a}_S$ and $\dot{\varepsilon}_{min}$ have different units. In the double logarithmic scales the $\dot{a}_S$–t_R and $\dot{\varepsilon}_{min}$–t_R relations are reasonably linear, insensitive to temperature. The power-law $\dot{a}_S$–t_R relation for the CCG tests and the power-law $\dot{\varepsilon}_{min}$–t_R relation for the uni-axial creep tests follow actually Monkman–Grant correlation

$$\dot{a}_S(\dot{\varepsilon}_{min}) \cdot t_R^{\beta_{MG}} = C_{MG}, \tag{11}$$

where C_{MG} and β_{MG} are constants. β_{MG} is 0.84 and 0.7 for the CCG tests and for the uni-axial creep tests, respectively.

3.3. Post test metallography

For the uni-axial creep tests necking appeared prior to the rupture. Transgranular rupture is dominant, see Fig. 13. No creep damage as cavity formation was observed. This is the case regardless of temperature and time.

For the CCG tests of the as-received material at 360 °C, deformed grains close to the crack and transgranular crack propagation were observed in the crack growth zone at higher stresses (shorter rupture times). At lower stresses (longer rapture times), hardly any deformation close to the crack was seen and the crack propagated intergranularly, characterised by rock pattern on the fracture surface, see Fig. 14.

For the CCG tests of the simulated CGHAZ the cracks propagated intergranularly, independent of temperature and time, see Fig. 15. Hardly any deformation adjacent to the crack was seen. Fractography

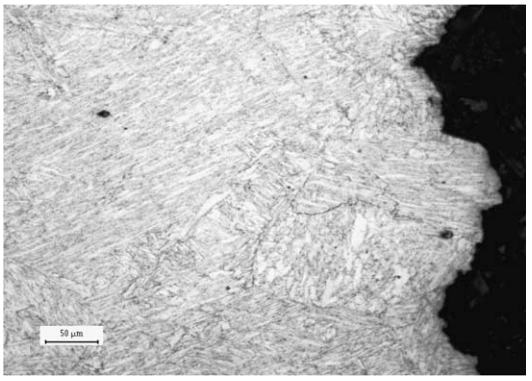

Fig. 13. LOM image showing fracture of uni-axial creep test on simulated CGHAZ failed after 19991 h at 320 °C and 715 MPa.

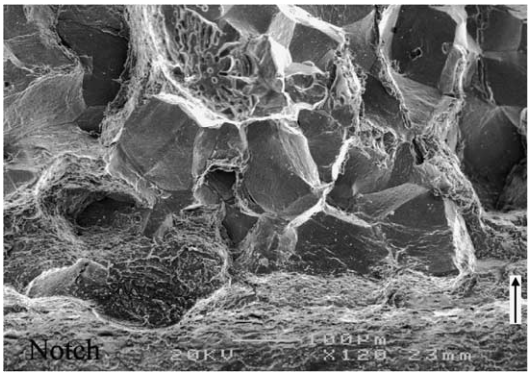

Fig. 14. SEM image showing fracture surface of CCG test on as-received material failed after 1211 h at 360 °C and 470 MPa. Arrow indicates crack propagation direction.

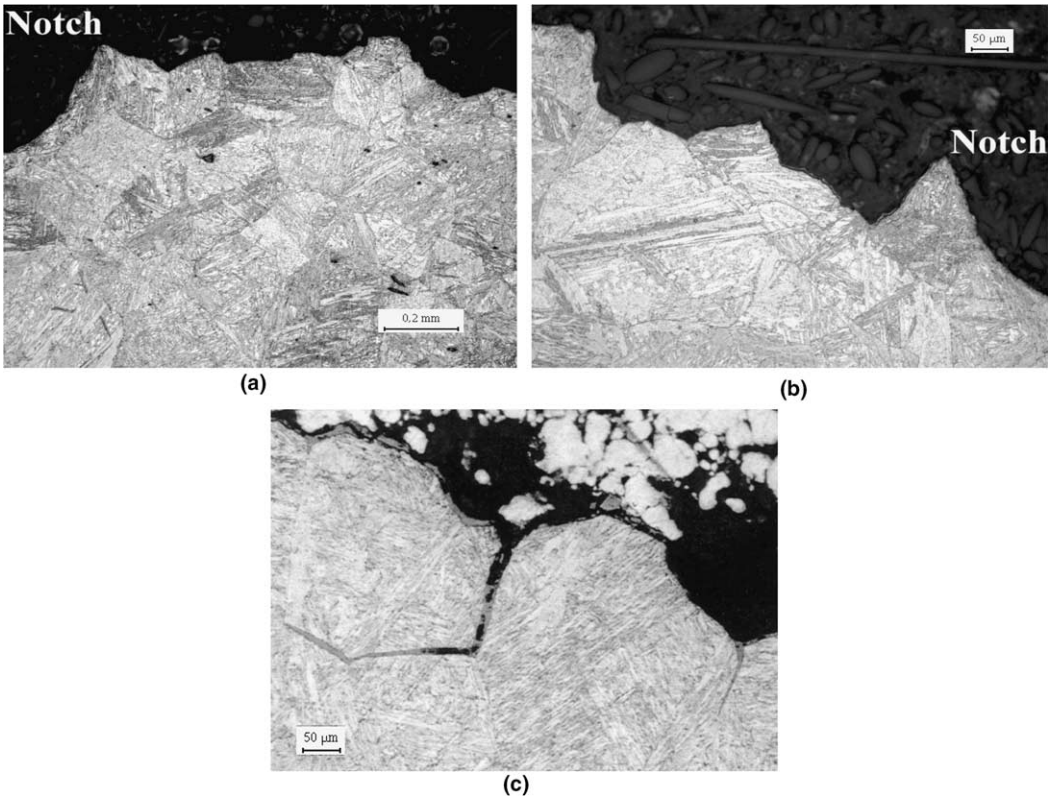

Fig. 15. LOM images showing fracture of CCG tests on simulated CGHAZ. (a) 320 °C/620 MPa/10907 h; (b) 340 °C/555 MPa/4156 h; (c) 420 °C/200 MPa/527 h.

examinations show also intergranular crack growth, characterised by rock pattern on the fracture surface, see Fig. 16. At longer rupture times at 420 °C the secondary cracks deviating from the main crack were seen to grow intergranularly, see Figs. 15(c) and 16(b).

4. Discussion

4.1. Uni-axial creep and creep crack growth tests

At higher stresses the difference in the time to rupture t_R for uni-axial and CCG tests is insignificant. However,

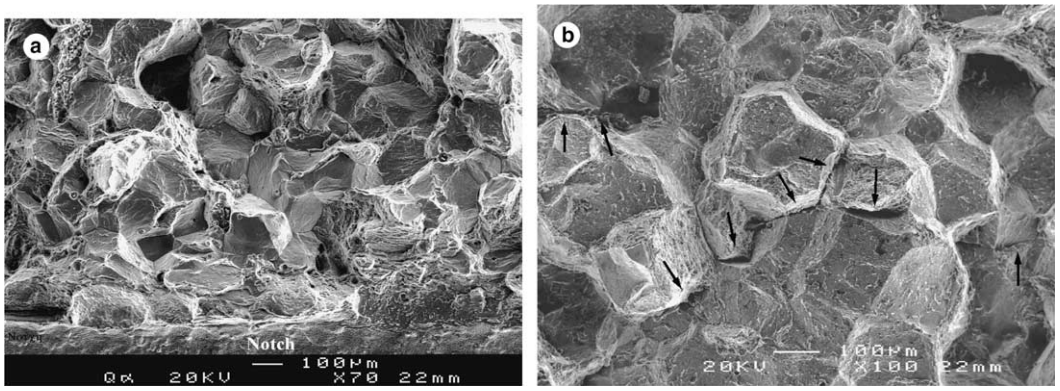

Fig. 16. SEM images showing fracture surface of CCG test on simulated CGHAZ. (a) 320 °C/620 MPa/10 907 h; (b) 420 °C/200 MPa/527 h. Arrows indicate secondary cracks.

this difference increases with increasing t_R, or decreasing stresses. At longer t_R (lower stresses), t_R for CCG tests is considerably shorter than that for uni-axial tests at the same temperature, see Fig. 4. Increasing temperature resulted in a shorter t_R for both uni-axial and CCG tests, see also Fig. 4 and a higher crack growth rate at the same reference stress σ_{ref} for the CCG tests, cf. Fig. 11, or a higher minimum creep strain rate at the same stress for the uni-axial creep test, cf. Fig. 6. Creep ductility in terms of elongation at rupture for the uni-axial tests is about 8%, independent of both temperature and time to rupture.

As-received ferritic–pearlitic material (Fig. 1(a)) transformed in the CGHAZ simulating heat treatment into tempered martensite (Fig. 1(b)). This results in a significant increase in both grain size and hardness. Gooch [7] has showed that the tempered martensite formed by quenching from 1050 °C is more crack resistant than the softer ferrite–pearlite in C–Mn steel, ascribing to the fine structure of the martensite and the absence of high energy ferrite–ferrite and ferrite–pearlite boundaries. This agrees with the present observations, in which the tempered martensite gives longer rupture times at higher stresses than the pearlite–ferrite, cf. series CCG360S and CCG360AR in Fig. 4. There is a tendency, however, that the pearlite–ferrite is more crack resistant than the tempered martensite at lower stresses.

No creep cavitation is visible and transgranular fracture is dominant for the uni-axial creep tests regardless of temperature and time to rupture, see Fig. 13. This is in agreement with previous studies [5,6]. Clearly, failure in the uni-axial creep tests is controlled by locally excessive plastic deformation leading to plastic collapse (necking and failure). For the CCG tests there is an obvious crack growth and the cracks propagate intergranularly, see Figs. 8, and 14, 15, 16. It seems that a sufficiently low reference stress with the accompanying relatively long testing time is required to facilitate crack growth. The longer the time to rupture, the larger the crack, see Fig. 10. The intergranular crack growth has been previously reported in [3,5,7]. Gooch [3] stated that for ferrite–pearlite structure in C–Mn steel the favoured paths for crack propagation are along ferrite–ferrite and ferrite-pearlite boundaries.

Studies of stress relief cracking of low alloy ferritic steels have demonstrated two fracture modes referred to as high temperature brittle intergranular fracture (HTBIF) and intergranular microvoid coalescence (IMC), see e.g. [14]. HTBIF is induced by stress segregation of impurity elements such as sulphur or phosphorus at the former austenite grain boundaries. If the material is tempered the tendency to HTBIF is strongly reduced. Although observed in the temperature range 300–600 °C, for low alloy steels HTBIF is primarily found in the upper end of this range. Below 450 °C crack growth is dominated by IMC both in the as quenched state and the tempered state. It is very unlikely that either HTBIF or IMC have appeared in the present study. For HTBIF (i) it would be outside its normal temperature range of observation, (ii) the studied simulated HAZ has been tempered, and (iii) results from materials with different sulphur content have not demonstrated any significant influence of the sulphur content. Concerning IMC no microvoid formation has been observed and this mechanism can consequently be ruled out.

It is clear that creep crack growth, rather than creep cavity formation, is the principal mechanism limiting the service performance of low alloy C–Mn steel around 300 °C. Therefore, understanding the behaviour of existed small crack, crack initiation and growth is essential in the nuclear power plants.

4.2. ASME E-1457 standard

The ASME standard E-1457 is used in many CCG tests and it is also adapted in the present study to provide a guideline for the experimental set-up, test

procedure, calculations of various parameters, and evaluations of results. In the E-1457 restrictions are imposed to determine when extensive creep has been reached. This depends on the relative amounts of elastic, plastic and creep deformation incurred at the crack tip. It has been demonstrated [15] for a material undergoing secondary creep that a steady state creep stress distribution is achieved after a transition time t_T given by

$$t_T = \frac{K_I^2}{(n+1)\cdot E\cdot C^*}, \tag{12}$$

where E is the elastic modulus. In the E-1457 all the data collected at times $t < t_T$ are considered as invalid. It can however be argued that a steady state creep stress distribution is achieved at a crack tip at an earlier time first when $t = t_T$ has been satisfied so that more data can be included. In the present case, assuming $K_I = 120\,\text{MPa m}^{1/2}$ and $C^* = 1\times10^{-5}$ MPa m/h, and using the values of n and E in Table 2, a rough estimation of t_T is 185 h at 320 °C and is 222 h at 340 °C, respectively. Many data points can therefore be regarded as valid, see Fig. 9.

To obtain a correlation of creep crack growth rate with C^*, it is necessary to achieve a steady state distribution of creep damage ahead of a crack tip as well as a steady state creep stress distribution [12]. The creep damage gradually builds up from the beginning of a test. This is a cause of the initial period of very little crack extension, which is referred to as an incubation period, see Fig. 7. In E-1457 it is implied that the incubation time is achieved after a crack extension of 0.5 mm. In the present study, the incubation time is empirically defined as $V/V_0 \approx 1.005$ and a continuous and consistent crack growth is followed thereafter. The corresponding crack length at $V/V_0 \approx 1.005$ is less than 0.2 mm, see Fig. 7. The use of a smaller crack length than 0.5 mm, e.g. 0.2 mm, has been proposed elsewhere [16].

4.3. Creep crack growth behaviour

Similar to the uni-axial creep curve where creep strain is plotted against time, see Fig. 3, the crack length increase as a function of time exhibits three distinct regions, see Fig. 7. There is an incubation period in which the crack is nearly stationary. After incubation, the crack starts to propagate steadily. The steady crack growth rate, which corresponds to the minimum creep strain rate, can be measured. Passing the steady growth region, crack growth becomes unstable, which corresponds to tertiary creep. Crack growth accelerates, leading to failure. An important aspect concerning the crack growth is that significant crack accumulation takes place at later stage of test and crack grows quickly.

The crack incubation time t_{in} prior to any significant crack advance can occupy a significant fraction of the total lifetime. For instance, t_{in} takes up more than 50% of total lifetime at 320 °C and about 20–30% of total lifetime in the most cases at other tested temperatures. Although the calculated t_{in} is reported elsewhere [12,17,18], t_{in} in the present study is empirically determined, see also Section 4.2. Empirically determined t_{in} has also been given in [5,19]. It is apparent that empirically determined t_{in} depends to a large extend on the accuracy of experimentally recorded values of V and V_0. In addition, the choice of V/V_0 as a measure of t_{in} must be established.

From Fig. 7 it is seen that the accumulated crack length prior to unstable crack growth in most cases is very small, e.g. less than 1 mm. Such small crack can be easily ignored in site inspection. This rises a warning in estimating life exhaustion governed mainly by creep crack growth process since small crack may accelerate rapidly and failure may appear unexpectedly. This is especially true in structural application where stress concentrations and bending forces occur.

4.4. Lifetime assessment

The ASME standard E-1457 test method characterises creep crack growth behaviour in terms of magnitude of a creep fracture parameter C^* under conditions of extensive creep deformation. In this case, C^* can be used to describe the local stress strain fields around a crack tip in a body subjected to creep. The relationship between creep crack growth rate and C^* can be utilised in the design and evaluation of engineering structures operated at creep conditions, see Fig. 9. The C^* value can be derived for a given crack with the help of finite element programs or approximate methods. Knowing the crack growth rate, the remaining lifetime can be predicted at given operating conditions by applying Eqs. (10) and (4), cf. Figs. 11 and 4, or by using Eq. (11), cf. Fig. 12.

A more direct approach is to make an approximate linear extrapolation based on the reference stress–time to rupture relation shown in Fig. 4 to estimate the lifetime. Since the absolute slope of creep rupture curves typically increases with increasing test time, the lifetime can be expected to be somewhat overestimated. The predicted lifetime represents a component with a small (mm-sized) crack [20]. Assuming a design lifetime of 100 000 h, the reference stress causing failure due to CCG in the coarse grained HAZ is 507 MPa at 320 °C, 362 MPa at 340 °C, 285 MPa at 360 °C, and 78 MPa at 420 °C, respectively. The reference stress causing failure of 100 000 h due to CCG in the as-received parent material is 416 MPa at 360 °C. The uni-axial creep stress causing failure of 100 000 h due to creep in the coarse grained HAZ is 682 MPa at 340 °C. The yield and tensile strengths are 614 and 756 MPa, respectively, at 320 °C, cf. Table 2. Although yield and tensile strength values

are not available at the other temperatures, they can all be expected to be considerable higher than the reference stresses for creep crack growth at the corresponding temperature. Apparently, the integrity of BWR and PWR nuclear reactor pressure vessel made of low alloy steel operating at around 300 °C is mainly controlled by creep crack growth in the HAZ.

There is a need to reconsider the design criterion for low alloy steels operating at temperature ranges originally defined below the limit temperature of 425475 °C. Stress causing failure by low temperature creep crack growth in the different microstructures must be taken into account, along with yield strength and tensile strength.

5. Conclusions

Uni-axial creep and creep crack growth (CCG) tests at 320–420 °C as well as post test metallography have been carried out on the as-received material and simulated CGHAZ of a low alloy reactor pressure vessel steel (ASTM A508 class 2). The following conclusions can be drawn:

1. The CCG does occur at temperatures between 320 °C and 420 °C. The material, especially for simulated CGHAZ, seems to be sensitive to cracks and defects.
2. The lifetimes for the CCG tests on the simulated CGHAZ are considerably shorter than those for the uni-axial creep tests at lower stresses.
3. Increasing temperature shortens both creep and CCG lifetimes significantly, e.g. the CCG lifetime on the simulated CGHAZ is reduced by a factor of five as temperature raises from 320 °C to 340 °C at given reference stresses. Incubation time and steady crack growth rate is decreased and increased, respectively, with increasing temperature.
4. For the CCG tests lifetimes on the simulated CGHAZ having tempered martensite were longer than those on as-received material having pearlite–ferrite at higher reference stresses. This tends to be reversed at lower reference stresses.
5. There are three regions when crack length is plotted against time, namely incubation, steady growth and instability. After incubation, in which crack is inactive, the crack starts to grow steadily. This is followed by unstable crack advance where crack growth accelerates, leading to rupture. Significant crack accumulation takes place at later stage of tests and the crack advances quickly.
6. For the uni-axial creep tests on the simulated CGHAZ no creep cavitation is observed and transgranular fracture is dominant. For the CCG tests at longer times, crack propagates intergranularly, regardless of microstructure and temperature.
7. The power-law relations between time to rupture and reference stress, between steady crack growth rate and reference stress (Norton's law for the uni-axial creep), and between steady crack growth rate and time to rupture (Monkman–Grant correlation for the uni-axial creep) are found for the CCG tests. These findings suggest potential application in life assessment for cases dominated by CCG.
8. Linear extrapolation based on log reference stress–log time to failure results that the reference stress causing failure on the simulated CGHAZ due to CCG at a given lifetime of 100 000 h at 320 °C is 507 MPa, clearly lower than both yield and tensile strengths, on which the design stress is typically based. Therefore, it is likely that the original design stress is not conservative or safe.

Acknowledgment

This work was carried out at the Swedish Institute for Metals Research. The Swedish Nuclear Power Inspectorate (SKI) is gratefully acknowledged for financial support. Vattenfall Energisystem is thanked for providing test material. The committee members, Xantopolous Konstantinos, SKI, Christer Jansson, Vattenfall Energisystem and Professor Kjell Pettersson, Matsafe AB, are greatly thanked for their discussions and comments.

Appendix A

$\dot{V}_c$ is calculated as follows

$$\dot{V}_c = \dot{V} - \frac{\dot{a}B_N}{P}\left(\frac{2K^2}{E'} + (m+1)J_p\right), \tag{A.1}$$

where $\dot{V}$ is the total load line displacement in mm/h. In the present case $\dot{V}$ is the same as LLD rate and has been experimentally recorded, $\dot{a}$ is the crack growth rate in mm/h, cf. Eq. (6). E' is equal to E for plane stress and E' is equal to $E/(1-\nu^2)$ for plane strain, where E is the elastic modulus in GPa and ν is the Poisson ratio. K is the stress intensity factor in MPa m$^{1/2}$. For CT specimens K is defined as

$$K = \frac{P}{\sqrt{B \cdot B_N \cdot W}} \cdot \frac{2 + a/W}{(1-a/W)^{3/2}} \cdot f(a/W), \tag{A.2}$$

where

$$f(a/W) = 0.866 + 4.64(a/W) - 13.32(a/W)^2 + 14.72(a/w)^3 - 5.6(a/W)^4. \tag{A.3}$$

The fully-plastic component of the J-integral, J_p, is given as follows

$$J_p = \frac{D_1 \cdot h_1 \cdot (a/W, m)}{(\sigma_{p0.2} \cdot (W-a))^m}\left(\frac{P}{1.455 \cdot B_N \cdot \beta}\right)^{m+1}, \tag{A.4}$$

$\sigma_{p0.2}$ is the yield stress in MPa. β, D_1, m and h_1 are the material constants. β is defined as follows

Table 3
Constants used in the C^* calculations

Temperature (°C)	Norton exponent n	h_1	E-modulus (GPa)	Yield stress $R_{p0.2}$ (MPa)	D_1	m
320	66	0.461	116.4	614	0.00429	10.27
340	89	0.388	72.37	614	0.0039	11.53

$$\beta = \sqrt{\Phi^2 + 2\Phi + 2} - (\Phi + 1), \tag{A.5}$$

where Φ is equal to

$$\Phi = \frac{2a}{(W - a)}. \tag{A.6}$$

D_1 and m are given in the Ramberg–Osgood stress–strain relation

$$\varepsilon = \frac{\sigma}{E} + D_1 \left(\frac{\sigma}{\sigma_{p0.2}}\right)^m. \tag{A.7}$$

The constant h_1 is a function of the ratio a/W and M and is tabulated in [9]. D_1 and m can be determined by carrying out tensile test at given temperature. In the present investigation the constants used in the C^* calculations at both 320 °C and 340 °C are listed in Table 3.

References

[1] G.J. Neate, Mater. Sci. Tech. 3 (1) (1987) 14.
[2] I.A. Shibli, Mater. Sci. Tech. 3 (2) (1987) 110.
[3] D.J. Gooch, Mater. Sci. Eng. 64 (2) (1984) 183.
[4] R. Sandström, G. Östberg, Creep failure below the limit temperature, Swedish Institute For Metals Research, 1M-2517, 1989.
[5] R. Wu, F. Seitisleam, R. Sandström, in: Proceedings of International Conference on Plant Maintenance For Managing Life and Performance, Baltica IV, Helsinki – Stockholm – Kirkkonummi, 7–9 September 1998, p. 623.
[6] J. Storesund, N. Tada, R. Sandström, On the notch sensitivity of creep failure below the limited temperature, 21st MPA-seminar, Stuttgart, 1995.
[7] D.J. Gooch, Mater. Sci. Eng. 83 (1) (1986) 17.
[8] Designation A508-54, standard specification for quenched and tempered vacuum-treated carbon and alloyed forgings for pressure vessels, Annual Books of ASTM Standards, 1985, p. 403.
[9] Designation ASTM E-1457-98, standard test method for measurement of creep crack growth rates in metals, draft version, 1998.
[10] K.H. Schwalbe, D.J. Hellman, Application of the electrical potential method to crack length measurements using Johnson's formula, Test. Evaluat. 9 (3) (1981) 218.
[11] H.H. Johnson, Mater. Res. Standards 5 (9) (1962) 442.
[12] G.A. Webster, R.A. Ainsworth, High Temperature Component Life Assessment, Chapman and Hall, London, 1994, ISBN 0 412 58520 0.
[13] K.M. Nikbin, D.J. Smith, G.A. Webster, Trans. ASME J. Eng. Mater. Technol. 108 (1986) 186.
[14] I.A. Vatter, C.E. Lane, Mater. Sci. Technol. 9 (10) (1993) 915.
[15] A. Saxena, J.D. Landes, in: Conference Proceedings of 6th International Conference on Fracture, Characterisation of Creep, Crack Growth in Metals, Advances in Fracture Research, Pergamon, 1984, p. 3977.
[16] Brite/Euram project, Be7463, Final report, Creep crack growth of C-Mn steels at 320 °C–400 °C, unpublished results, 1998.
[17] H. Riedel, J.R. Rice, in: Fracture Mechanics 12 Conference, ASTM Spec. Tech. Publ. 700 (1980) 112.
[18] R.A. Ainsworth, M.C. Coleman, Fatigue Fract. Eng. Mater. Struct. 10 (2) (1987) 129.
[19] I.A. Shibli, Low temperature (360 °C) creep crack growth characteristics of C–Mn steel, Mater. Sci. Eng. A 104 (1988) 29.
[20] R. Wu, F. Seitisleam, R. Sandström, Key Eng. Mater. (Switzerland) 171–174 (2000) 139.